Matthias Sabel
Institute of Applied Mechanics,
University of Kaiserslautern,
Kaiserslautern 67663, Germany
e-mail: msabel@rhrk.uni-kl.de

Christian Sator
Institute of Applied Mechanics,
University of Kaiserslautern,
Kaiserslautern 67663, Germany

Tarek I. Zohdi
Computational Mechanics Research Laboratory,
University of California, Berkeley,
Berkeley, CA 94720-1740

Ralf Müller
Institute of Applied Mechanics,
University of Kaiserslautern,
Kaiserslautern 67663, Germany
e-mail: ram@rhrk.uni-kl.de

Application of the Particle Finite Element Method in Machining Simulation Discussion of the Alpha-Shape Method in the Context of Strength of Materials

In particle finite element simulations, a continuous body is represented by a set of particles that carry all physical information of the body, such as the deformation. In order to form this body, the boundary of the particle set needs to be determined. This is accomplished by the α-shape method, where the crucial parameter α controls the level of detail of the detected shape. However, in solid mechanics, it can be observed that α has an influence on the structural integrity as well. In this paper, we study a single boundary segment of a body during a deformation and it is shown that α can be interpreted as the maximum stretch of this segment. On the continuum level, a relation between α and the eigenvalues of the right Cauchy–Green tensor is presented. [DOI: 10.1115/1.4034434]

1 The Particle Finite Element Method (PFEM)

Common techniques in computational modeling can be categorized as continuum based or discrete methods. Discrete methods, such as molecular dynamics are well suited to track large configurational changes and can therefore determine, e.g., the nucleation and growth of defects. However, these methods are computationally expensive for problems with large length- and time-scales. Standard finite element methods (FEMs) are a common way to solve continuum-based problems and are well established in various engineering applications. Although they are well suited to model problems on the scale of engineering components, large configurational changes often lead to a failure of the method. The particle finite element method (PFEM) combines the benefits of continuous and discrete methods and is, therefore, well suited to cope with large configurational changes, e.g., separation of material. It was first applied to problems with sloshing liquids in Ref. [1], and since then the number of applications has increased including problems in solid mechanics as in Refs. [2,3] or even simulations of liquid–solid interaction in Ref. [4]. The PFEM algorithm used in this work consists of several parts. At first, the boundary of a set of particles needs to be determined which is accomplished by the so called α-shape method. This method originates from the field of computer graphics (see e.g., Refs. [5,6]) and will be explained in more detail in Sec. 2. After detecting the boundary, the region can be meshed with finite elements. A detailed description of the element implementation used in this work, will be given in Sec. 3. After the meshing, a FEM problem can be solved, where the deformation data of previous load steps needs to be included to restore the overall deformation. The FEM problem is then solved using the academic code FEAP [7], the resulting displacements are used to update the particle coordinates, and the deformation gradient is stored for the next load step. Figure 1 gives a graphic overview of the algorithm.

2 Identifying the Boundary

The boundary of a set of particles S can be considered as a chain of boundary segments. To identify these segments, every possible pair of particles within the set needs to be examined. A two-dimensional ball (or circle) that intersects the respective pair is defined and it is tested, if the circle contains any other particles of the set. The radius of this circle corresponds to the minimum distance between any two particles in the set, scaled by the parameter α. If no other particles are located in the circle, the line between the respective pair forms a boundary segment. Therefore, it can be said that there are two essential conditions which have to be fulfilled in order to form a boundary segment. The distance between the pair of particles must not exceed the diameter of the circle and the circle must not contain any other particles. In the following paragraph, the working principle of the α-shape method is explained in more detail.

Consider two particles i and j as displayed in Fig. 2 which are part of the set S.

The line element connecting these particles is then described as the vector

```
input  : particle coordinates, deformation gradient
output: updated coordinates and gradients
for i = 1 to number of load steps do
    read particle coordinates
    detect boundary
    mesh region
    if i > 1 then
        include deformation gradients of step i − 1
    end
    solve FE problem
    update particle coordinates
    save current gradients
end
```

Fig. 1 PFEM algorithm in pseudocode

Contributed by the Design Engineering Division of ASME for publication in the Journal of Computing and Information Science in Engineering. Manuscript received September 23, 2015; final manuscript received August 4, 2016; published online November 7, 2016. Editor: Bahram Ravani.

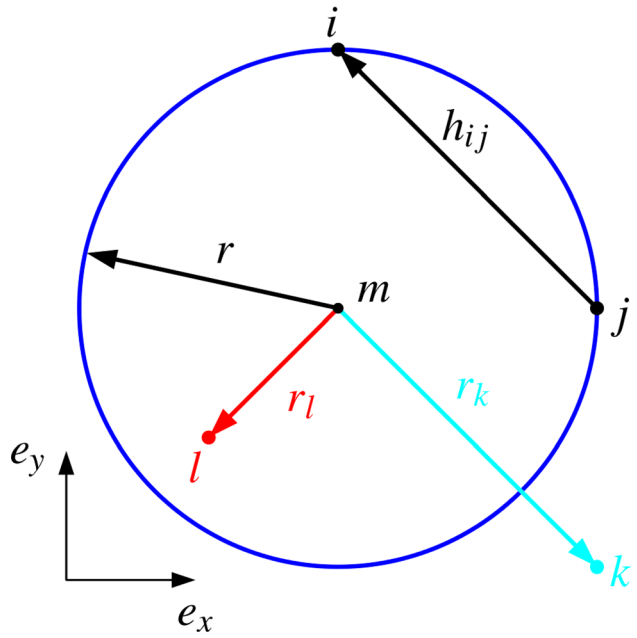

Fig. 2 Detecting segments between particles

$$\boldsymbol{h}_{ij} = \boldsymbol{x}_i - \boldsymbol{x}_j \tag{1}$$

In order to define a circle intersecting both particles, we need to define the direction to the midpoint of the circle. This is realized with an orthogonal vector to the line segment

$$\boldsymbol{n}_{ij} = \frac{1}{|\boldsymbol{h}_{ij}|} \begin{pmatrix} - \boldsymbol{h}_{ij} \cdot \boldsymbol{e}_y \\ \boldsymbol{h}_{ij} \cdot \boldsymbol{e}_x \end{pmatrix} \tag{2}$$

This vector is normalized and has to be scaled to give the accurate position of the circle's center. Making use of Pythagoras's theorem, this value can be expressed as

$$d = \sqrt{r^2 - \left(\frac{1}{2}|\boldsymbol{h}_{ij}|\right)^2} \tag{3}$$

where the radius of the circle is defined as

$$r = \alpha\, h_{\min} \tag{4}$$

In Eq. (4), $h_{\min}$ symbolizes the minimum distance between any two particles in the set S. With the distance d from the circle's center to the vector $\boldsymbol{h}_{ij}$, the position of the midpoint as shown in Fig. 2 can be expressed as

$$\boldsymbol{m}_{ij} = \frac{1}{2}(\boldsymbol{x}_i + \boldsymbol{x}_j) + d\,\boldsymbol{n}_{ij} \tag{5}$$

The final step of the method is to examine if any other particles are located in the circle. For an arbitrary particle k, its distance to the center of the circle can be defined as

$$|\boldsymbol{r}_k| = |\boldsymbol{x}_k - \boldsymbol{m}_{ij}| \tag{6}$$

If the condition $|\boldsymbol{r}_k| \geq r$ is fulfilled, particle k is not located within the circle and the condition is checked for every remaining particle in the set S. If the condition holds, particles i and j form a boundary segment. In Fig. 3, two examples of a detected boundary for the same set of particles are shown.

From the figures, it can be easily observed that different values for α lead to different boundaries. The boundary on the left is detected with $\alpha = 1.0$ and the boundary on the right is detected with $\alpha = 2.0$, where the small notch is not captured and the larger notch is shaped differently. This indicates that the choice of α controls the level of detail and is therefore highly significant.

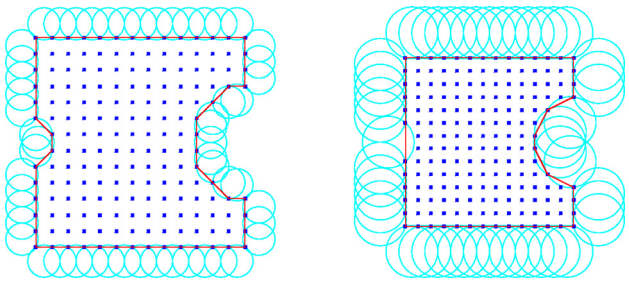

Fig. 3 Result of boundary detection for $\alpha = 1.0$ and $\alpha = 2.0$

3 Solution of Boundary Value Problems and Update of Particle Data

After identifying the boundary, a continuous body can be defined. Combined with boundary conditions, we can state a boundary value problem using the basic equations of nonlinear solid mechanics. These are taken from textbooks as Refs. [8–10]. Since we want to track the changes in the topology, we divide the overall mechanical load into several load steps, and redetect the boundary in between these steps. This means that the overall deformation is defined as

$$\boldsymbol{F} = \frac{\partial \boldsymbol{x}}{\partial \boldsymbol{X}} = \frac{\partial \boldsymbol{x}}{\partial \boldsymbol{\xi}} \frac{\partial \boldsymbol{\xi}}{\partial \boldsymbol{X}} = \boldsymbol{F}^{\text{act}}\, \boldsymbol{F}^{\text{old}} \tag{7}$$

The coordinate $\boldsymbol{\xi}$ then describes the position of the body in one of the load steps, and the coordinates $\boldsymbol{X}$ and $\boldsymbol{x}$ represent the position in the undeformed, and deformed configuration. This multiplicative split of the deformation gradient can be found in Ref. [11] and goes back to Ref. [12], where it was first used in the context of elastoplasticity. Using this modified deformation gradient, we can compute the left Cauchy–Green tensor to express the strain in the current configuration

$$\boldsymbol{b} = \boldsymbol{F}\boldsymbol{F}^{\mathrm{T}} \tag{8}$$

As constitutive relation, a hyperelastic material is considered and the stress in the actual configuration can therefore be expressed as

$$\boldsymbol{\sigma} = 2\boldsymbol{b}\frac{\partial W}{\partial \boldsymbol{b}} \quad \text{with} \quad W(\boldsymbol{b}) = \frac{\mu}{2}(I_B - 3) + g(J) \tag{9}$$

where the strain energy function W represents a standard neo-Hooke material and is based on the first invariant $I_B = \mathrm{tr}(b)$, and the determinant of the deformation gradient $J = \det \boldsymbol{F}$. The volumetric part of the strain energy function $g(J)$ is expressed as

$$g(J) = \frac{\lambda}{4}(J^2 - 1) - \frac{\lambda}{2}\ln J - \mu \ln J \tag{10}$$

and the parameters μ and λ in Eq. (10) represent the Lamé constants in the small deformation limit. For the current configuration, the mechanical equilibrium is defined using the Cauchy stress tensor

$$\mathrm{div}\,\boldsymbol{\sigma} + \boldsymbol{f} = \boldsymbol{0} \tag{11}$$

where $\boldsymbol{f}$ represents the volume forces and the divergence is computed with respect to $\boldsymbol{x}$. Now, all necessary equations have been stated and with boundary conditions we can form a boundary value problem. In order to solve the resulting problem, Eq. (11) is

transferred into a weak form which has to be linearized and discretized. For all problems discussed in this work, we use triangular finite elements with the shape functions

$$N_1(r,s) = 1 - r - s, \quad N_2(r,s) = r, \quad N_3(r,s) = s \tag{12}$$

where r and s are the element coordinates. After solving the finite element problem, the deformation gradient is projected from the Gauß points to the nodes. Before the final projection, improved values for the deformation gradient at the Gauß points

$$\boldsymbol{F}^{\mathrm{GP,impr}} = \sum_{I=1}^{N} N_I\left(r^{\mathrm{GP}}, s^{\mathrm{GP}}\right)\boldsymbol{F}^I \tag{13}$$

are calculated in a least squares sense. To obtain the final nodal values of the deformation gradient, the integral of the mesh volume

$$M_{IJ} = \int_{\mathcal{B}_t} N_I\left(r^{\mathrm{GP}}, s^{\mathrm{GP}}\right) N_J\left(r^{\mathrm{GP}}, s^{\mathrm{GP}}\right) d\Omega \tag{14}$$

and the entries of the deformation gradient on the element level weighted by the element volume

$$P_I(\boldsymbol{F}^{\mathrm{GP}}) = \int_{\mathcal{B}_t} N_I\left(r^{\mathrm{GP}}, s^{\mathrm{GP}}\right)\boldsymbol{F}^{\mathrm{GP}}\, d\Omega \tag{15}$$

have to be assembled, which leads to the set of linear equations

$$\sum_{J=1}^{N} M^{IJ}\boldsymbol{F}^J = P_I(\boldsymbol{F}^{\mathrm{GP}}) \tag{16}$$

The matrix M^{IJ} is diagonalized

$$\bar{M}_{II} = \sum_{J=1}^{N} M_{IJ} = \int_{\mathcal{B}_t} N_I\left(r^{\mathrm{GP}}, s^{\mathrm{GP}}\right) d\Omega \tag{17}$$

and the lumped system

$$\bar{M}^{II}\boldsymbol{F}^I = P_I(\boldsymbol{F}^{\mathrm{GP}}) \tag{18}$$

can easily be solved. In the next step, the old deformation data can be recaptured as

$$\boldsymbol{F}^{\mathrm{old}} = \sum_{I=1}^{N} N_I(r^{\mathrm{GP}}, s^{\mathrm{GP}})\boldsymbol{F}^{I,\mathrm{old}} \tag{19}$$

and the overall deformation can be recovered using Eq. (7).

4 Physical Interpretation of α

As described in Sec. 2, the α-shape method detects the surrounding of a set of particles by identifying a path of segments connecting the boundary particles. Once the boundary of the body is established, the domain can be meshed and a finite element simulation is performed. After the simulation, the particle coordinates are updated by the displacements. Now, the α-shape algorithm runs again and determines the boundary. Since the distances between particles change during a deformation, the detected boundary might change and recalling the working principle of the α-shape method, we can define two necessary conditions to identify a boundary segment. As mentioned in Sec. 2, an intersecting circle with the radius $r = \alpha h_{\min}$ is defined for every pairwise combination of particles in a set. This implies that the distance between these particles and therefore, the length of the segment must not exceed the diameter of the circle. Another necessary condition for the identification of boundary segments is that the circle must not contain any other particles. This confines the first condition w.l.o.g. to be valid only for segments at the boundary. In the following, the behavior of a boundary segment during a deformation is studied in order to investigate the relationship between the parameter α and a separation of material, i.e., failure of boundary segments. Figure 4 shows two particles i and j, and the related boundary segment before and after a deformation, as well as the corresponding α-circles.

In the undeformed state, the segment is of length $|\boldsymbol{H}|$ and is therefore smaller than the diameter $2\,\alpha\,|\boldsymbol{H}|$ of the circle. After a deformation Φ, the length of the segment and the diameter are equal, which gives a critical deformation for the case that $\boldsymbol{h}_{ij}$ is still a boundary segment. This critical point can be identified as

$$|\boldsymbol{h}| = 2\,\alpha\,|\boldsymbol{H}| \quad \rightarrow \quad \alpha = \frac{|\boldsymbol{h}|}{2\,|\boldsymbol{H}|} \tag{20}$$

Equation (20) implies that α can be interpreted as a critical stretch of a boundary segment. Since the PFEM is a combination of a discrete and a continuum-based modeling technique, it would be useful to establish a relation between the parameter α and the strain state in the continuous body in the sense of a failure criterion. Therefore, we express the length of the segments in Eq. (20) with the scalar product, which yields

$$(\boldsymbol{h}\cdot\boldsymbol{h})^{\frac{1}{2}} = 2\,\alpha(\boldsymbol{H}\cdot\boldsymbol{H})^{\frac{1}{2}} \tag{21}$$

From textbooks like Ref. [8] or [11], we know that the deformation of a line segment can be described with the mapping

$$\boldsymbol{h} = \boldsymbol{F}\,\boldsymbol{H} \tag{22}$$

where $\boldsymbol{F}$ is the deformation gradient. It must be noted that we assume $\boldsymbol{F}$ to be spatially constant. With this expression, we can eliminate the deformed segment $\boldsymbol{h}$ and rearrange Eq. (21) to

$$(\boldsymbol{F}\,\boldsymbol{H})\cdot(\boldsymbol{F}\,\boldsymbol{H}) = 4\,\alpha^2\,\boldsymbol{H}\cdot\boldsymbol{H} \tag{23}$$

Introducing the right Cauchy–Green tensor

$$\boldsymbol{C} = \boldsymbol{F}^{\mathrm{T}}\boldsymbol{F} \tag{24}$$

and with some transformations, we can express Eq. (23) as

$$\boldsymbol{H}\cdot((\boldsymbol{C} - 4\,\alpha^2\,1)\boldsymbol{H}) = 0 \tag{25}$$

In order to solve this equation, we transfer the right Cauchy–Green tensor into a diagonalized matrix

$$\mathrm{diag}(\lambda_i^C) = \boldsymbol{Q}^{\mathrm{T}}\boldsymbol{C}\boldsymbol{Q} \tag{26}$$

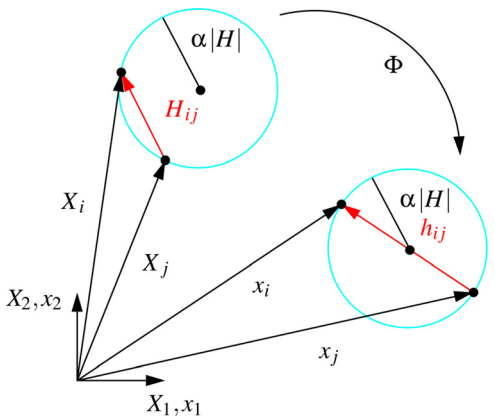

Fig. 4 Line element in reference- and spatial-configuration

where $\boldsymbol{Q}$ is an orthogonal matrix containing the eigenvectors of $\boldsymbol{C}$ corresponding to the eigenvalues λ_i^C. Equation (25) then becomes

$$\boldsymbol{H} \cdot ((\boldsymbol{Q}\boldsymbol{Q}^{\mathrm{T}}\boldsymbol{C}\boldsymbol{Q}\boldsymbol{Q}^{\mathrm{T}} - 4\,\alpha^2\,\boldsymbol{Q}\boldsymbol{Q}^{\mathrm{T}}1\boldsymbol{Q}\boldsymbol{Q}^{\mathrm{T}})\boldsymbol{H}) = 0 \tag{27}$$

which can be rearranged to

$$(\boldsymbol{Q}^{\mathrm{T}}\boldsymbol{H}) \cdot ((\mathrm{diag}(\lambda_i^C) - 4\,\alpha^2\,\mathbf{1})(\boldsymbol{Q}^{\mathrm{T}}\boldsymbol{H})) = 0 \tag{28}$$

Using the abbreviations $\boldsymbol{y} = \boldsymbol{Q}^{\mathrm{T}}\boldsymbol{H}$ and $\boldsymbol{A} = \mathrm{diag}(\lambda_i^C) - 4\,\alpha^2\,\mathbf{1}$, we can distinguish between three different solutions for the equation

$$\boldsymbol{y} \cdot (\boldsymbol{A}\boldsymbol{y}) = 0 \tag{29}$$

If tensor $\boldsymbol{A}$ is positive-definite ($\lambda_i^C > 4\alpha^2$) or negative-definite ($\lambda_i^C < 4\alpha^2$), only the trivial solutions $\boldsymbol{y}_i = \boldsymbol{0}$ exist, and therefore, the corresponding undeformed line segments are $\boldsymbol{H}_i = \boldsymbol{Q}\,\boldsymbol{y}_i = \boldsymbol{0}$.

If $\boldsymbol{A}$ is positive-semidefinite

$$(\lambda_1^C = 4\alpha^2 \wedge \lambda_2^C > 4\alpha^2 \quad \text{or} \quad \lambda_2^C = 4\alpha^2 \wedge \lambda_1^C > 4\alpha^2)$$

or negative-semidefinite

$$(\lambda_1^C = 4\alpha^2 \wedge \lambda_2^C < 4\alpha^2 \quad \text{or} \quad \lambda_2^C = 4\alpha^2 \wedge \lambda_1^C < 4\alpha^2)$$

the shape of the nontrivial solutions is

$$\boldsymbol{y}_1 = \begin{pmatrix} \kappa \\ 0 \end{pmatrix} \quad \boldsymbol{y}_2 = \begin{pmatrix} 0 \\ \kappa \end{pmatrix} \quad (\kappa \neq 0) \tag{30}$$

and the corresponding line segments are

$$\boldsymbol{H}_1 = \boldsymbol{Q}\,\boldsymbol{y}_1 = \kappa \begin{pmatrix} Q_{11} \\ Q_{21} \end{pmatrix}, \quad \boldsymbol{H}_2 = \boldsymbol{Q}\,\boldsymbol{y}_2 = \kappa \begin{pmatrix} Q_{12} \\ Q_{22} \end{pmatrix} \tag{31}$$

It should be noted that this would mean that the undeformed line segment $\boldsymbol{H}$ would have to be collinear to the eigenvectors corresponding to λ_i.

In the third case, $\boldsymbol{A}$ is indefinite

$$(\lambda_1^C > 4\alpha^2 \wedge \lambda_2^C < 4\alpha^2 \quad \text{or} \quad \lambda_2^C > 4\alpha^2 \wedge \lambda_1^C < 4\alpha^2)$$

The shape of the solution is

$$\begin{aligned} \boldsymbol{y}_1 &= \kappa \begin{pmatrix} \sqrt{-(\lambda_2^C - 4\alpha^2)} \\ \sqrt{\lambda_1^C - 4\alpha^2} \end{pmatrix} \\ \boldsymbol{y}_2 &= \kappa \begin{pmatrix} \sqrt{\lambda_2^C - 4\alpha^2} \\ \sqrt{-(\lambda_1^C - 4\alpha^2)} \end{pmatrix} \end{aligned} \tag{32}$$

and the undeformed line segment is

$$\boldsymbol{H}_1 = \boldsymbol{Q}\,\boldsymbol{y}_1 \quad \text{or} \quad \boldsymbol{H}_2 = \boldsymbol{Q}\,\boldsymbol{y}_2 \tag{33}$$

5 Analytical Example

In this section, the previous discussed theory is tested on a simple analytical example. The punched strip in Fig. 5 is a popular example in continuum mechanics and if subjected to a tensile loading, we expect the strip to fracture at the right and left boundary of the hole. As a first approach, a single finite element at the critical position of the boundary is studied. For this investigation, the element nodes are fixed in both degrees-of-freedom and a displacement $\hat{\boldsymbol{u}}$ is applied at the top node. The α-shape algorithm is applied to the blue-colored boundary segment and traces the separation of material.

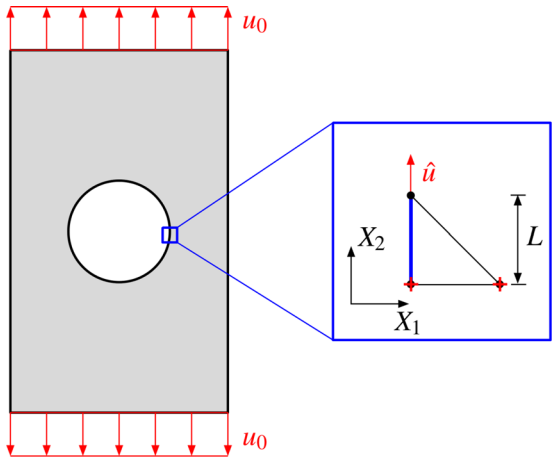

Fig. 5 Punched strip and critical boundary segment

The triangular finite element used in this work has already been briefly introduced in Sec. 3. For isoparametric elements, the deformation gradient can be expressed in terms of the transformation matrices

$$\boldsymbol{F}_e = \boldsymbol{j}_e\,\boldsymbol{J}_e^{-1} \tag{34}$$

where $\boldsymbol{j}$ maps the position vector in the deformed configuration to the isoparametric reference configuration and is defined as

$$\boldsymbol{j}_e = \frac{\partial \boldsymbol{x}}{\partial \boldsymbol{r}} = \sum_{I=1}^{N} \boldsymbol{x}_I \otimes \nabla_r N_I \tag{35}$$

In Eq. (35), $\boldsymbol{r}$ represents the coordinates in the isoparametric reference configuration and N_I are the shape functions described in Eq. (12). The transformation matrix $\boldsymbol{J}$ maps the position vector in the undeformed configuration to the isoparametric reference configuration. Hence, $\boldsymbol{J}$ is defined in a similar way as

$$\boldsymbol{J}_e = \frac{\partial \boldsymbol{X}}{\partial \boldsymbol{r}} = \sum_{I=1}^{N} \boldsymbol{X}_I \otimes \nabla_r N_I \tag{36}$$

Now, the right Cauchy–Green tensor can be formed according to Eq. (24) and the strain state is known in the finite element. The eigenvalues of $\boldsymbol{C}$ can be computed and compared to the limit $4\,\alpha^2$, which is presented in Fig. 6.

In Fig. 6, the maximum eigenvalue of $\boldsymbol{C}$ is plotted over the vertical stretch of the finite element. In this example, $\alpha = 1.0$ which represents a stretch of the boundary segment by 100%. If the maximum eigenvalue $\lambda_C > 4.0$, the α-circles at the segment cannot intersect both particles, and the segment fails.

6 Numerical Examples

Section 5 demonstrated the relation between α and the eigenvalues of $\boldsymbol{C}$ on an analytical example. Now, more sophisticated examples with a larger number of particles will be studied. The first three examples are bodies with simple geometries, subjected either to uniaxial tension or a shear deformation. Figure 7 demonstrates the two loading scenarios.

For the following examples subjected to a uniaxial tensile loading, the body is vertically fixed at the bottom and a vertical displacement is applied at the top. The simple shear simulation is carried out in a way that the left and right boundaries of the body are translated with linear decreasing displacements from top to

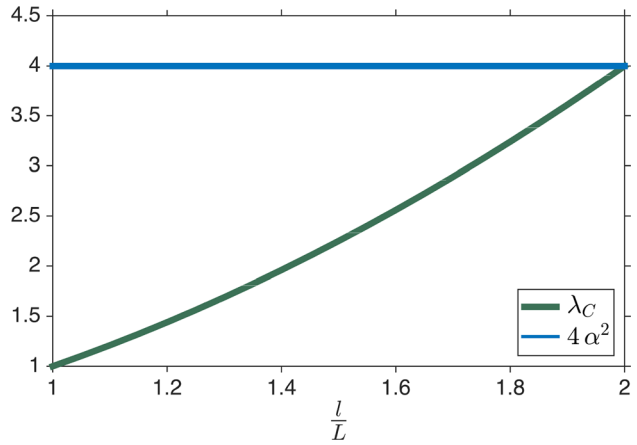

Fig. 6 Maximum eigenvalue compared to α-limit for $\alpha = 1.0$

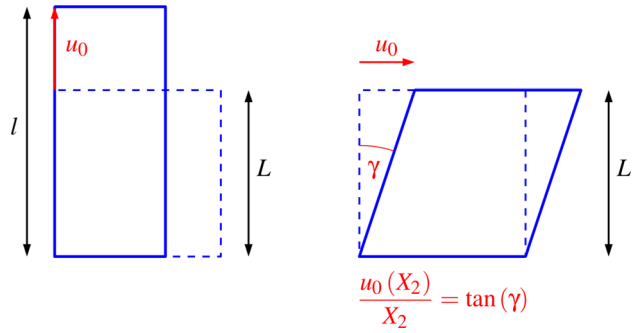

Fig. 7 Dimensions and displacements for uniaxial tension and simple shear simulations

bottom. The sides are then tilted by the shear angle γ as described in Fig. 7. Figure 8 shows the deformed body of the tensile test in the critical load step.

The contour plot in Fig. 8 represents the maximum eigenvalue at the Gauß points. For this simulation we set $\alpha = 1$, which means that the material separates if the maximum eigenvalue exceeds the value of 4. The figure displays the last load step, before the material separates. In the following simulation, the body is subjected to a simple shear loading scenario, and Fig. 9 shows a contour plot of the maximum eigenvalue.

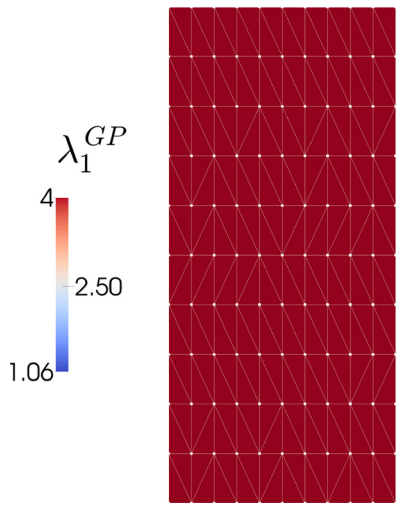

Fig. 8 Specimen under uniaxial tension

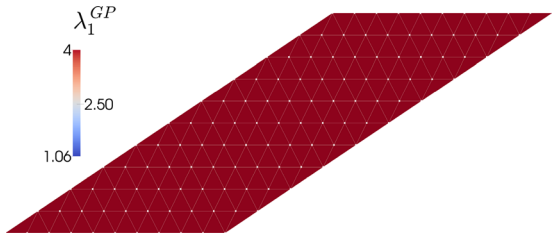

Fig. 9 Maximum eigenvalue in simple shear simulation

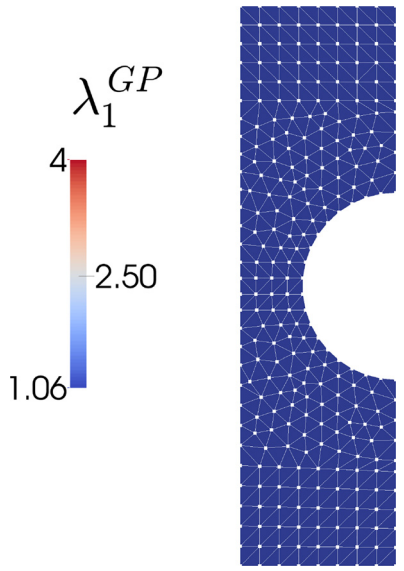

Fig. 10 Punched strip in undeformed setting

The body is again displayed in the critical load step where the maximum eigenvalue has just reached the critical point. This simulation was also carried out for $\alpha = 1.0$, which represents a maximum stretch of the boundary segments by 100%. In the next example, we again study the punched strip discussed in Sec. 5. The boundary conditions correspond to the ones used in the tensile test simulations, explained in Fig. 7. In Fig. 10, the punched strip is shown in the undeformed setting and the color code again indicates the maximum eigenvalue. As previously mentioned, the largest strain occurs at the middle of the punch hole, which is why we expect the material separation to start at this position.

Figure 11 shows a contour plot of the maximum eigenvalue in a latter load step. As expected, the specimen fails at the predicted position and at the critical eigenvalue corresponding to $\alpha = 1.0$.

To give more quantitative results, we studied the failure of the first boundary segment for the uniaxial tension, the simple shear, and the punched strip simulation. Figures 12–14 show the critical stretch of the boundary segments α and the ratio of the length of the deformed boundary segment with respect to the length of the undeformed segment for the three simulations.

In Figs. 12–14, the stretch of the boundary segment is plotted over the ratio of the size of the deformed specimen l and the size of the undeformed specimen L as displayed in Fig. 7 for the tensile test. For the case of the simple shear simulation, the ratio l/L is expressed as $l/L = 1 + \tan(\gamma)$ where the shear angle γ is explained in Fig. 7. The plots confirm the statement of the maximum stretch based on α and the first failure of a boundary segments occurs at the predicted point except for the simple shear simulation. The cause of this can be explained with Fig. 15.

Recalling the two conditions which need to be fulfilled in order to identify a boundary segment, one statement expresses that the α-circles must not contain any particles except for the ones that

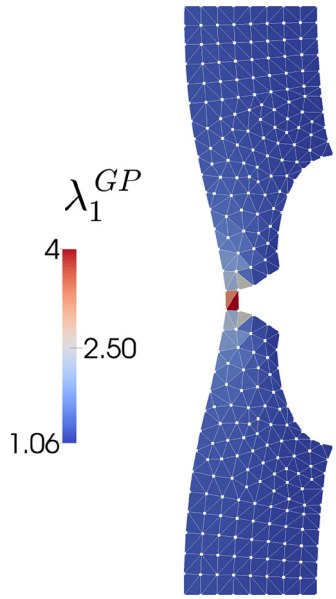

Fig. 11 Maximum eigenvalue plotted on deformed configuration

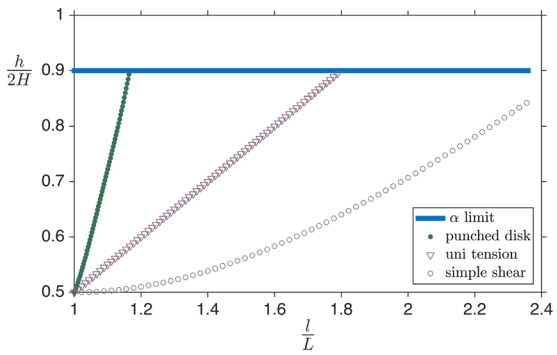

Fig. 12 Stretch of boundary segments *h*/*H* and critical stretch $\alpha = 0.9$

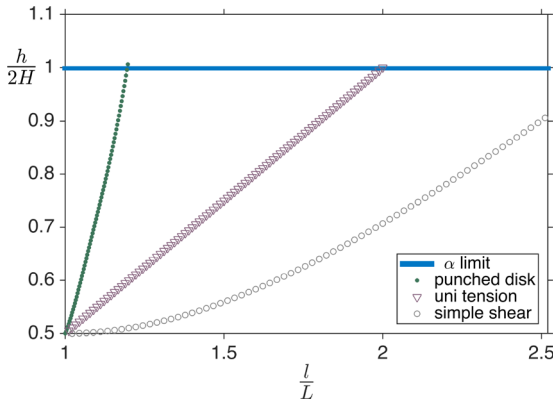

Fig. 13 Stretch of boundary segments *h*/*H* and critical stretch $\alpha = 1.0$

form the segment. However, in simulations with large deformations, the boundary may be strongly distorted and other particles move into the α-circles. On the left in Fig. 15, some particles are about to enter the α-circles. The right side of the figure shows the following load step where some former boundary segments have been eliminated, due to the violation of the mentioned condition.

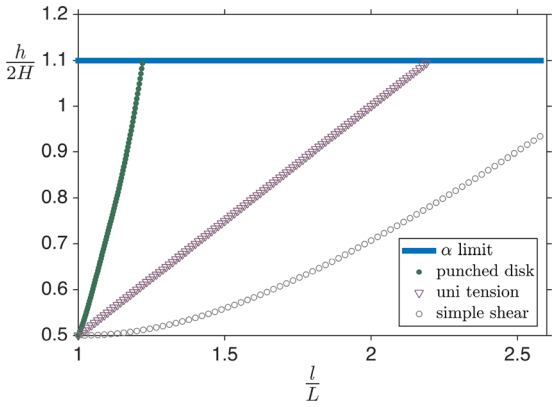

Fig. 14 Stretch of boundary segments *h*/*H* and critical stretch $\alpha = 1.1$

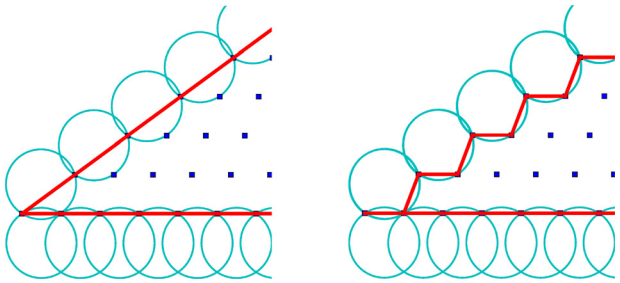

Fig. 15 Boundary segments and α-circles before and after separation

6.1 Applications in Manufacturing. As discussed in the introduction of this work, the PFEM was designed to cope with large configurational changes. In many processes in manufacturing, a material is largely deformed or separated. This section shows two applications in manufacturing. Since this implementation of the PFEM uses a hyperelastic material model, the material parameters for these simulations were set to $\mu = 925\,\text{MPa}$ and $\lambda = 2160\,\text{MPa}$, which mimics the behavior of plastics. The first numerical example is a simulation of a vertical cutting process, where a workpiece is shortened by a cutting tool. Figure 16 shows the workpiece represented by a set of particles and the rigid tool.

In this simulation, only the left part of the workpiece is fixed in both degrees-of-freedom. The cutting tool is vertically translated and a normal contact condition is considered between tool and workpiece. Figure 16 shows the maximum eigenvalue at Gauß point level and it can be observed that the material separates in a region with high stretches. However, this simulation is done with $\alpha = 0.8$, and therefore, the predicted critical eigenvalue is 2.56.

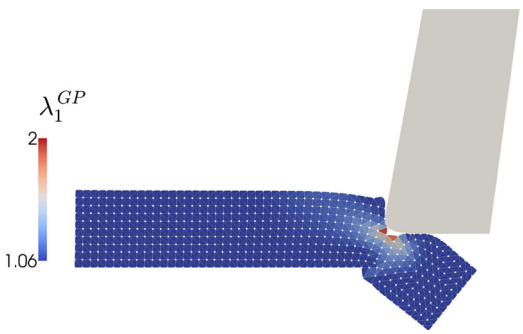

Fig. 16 Maximum eigenvalues in workpiece for $\alpha = 0.8$

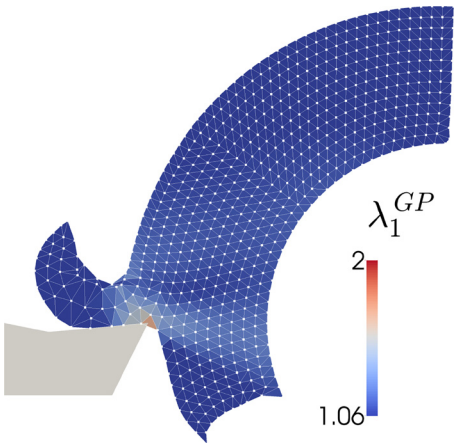

Fig. 17 Turning simulation for $\alpha = 1.0$

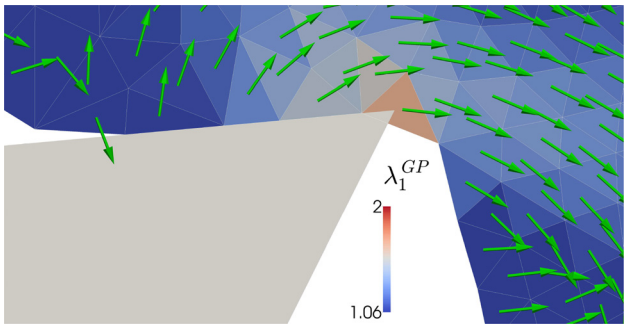

Fig. 18 Maximum eigenvalues and corresponding eigenvectors

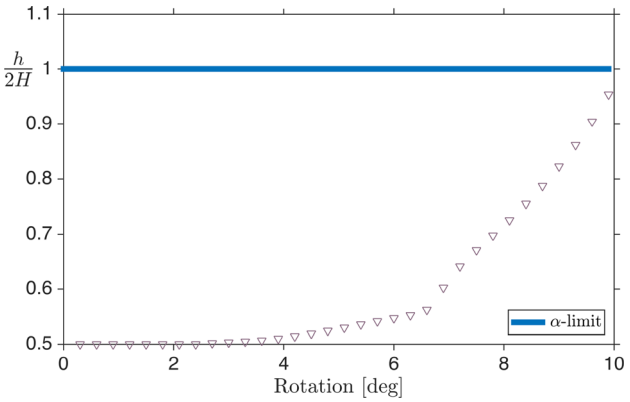

Fig. 19 Stretch of boundary segment compared to α

The color code indicates that the actual eigenvalues are somehow smaller than the critical value, which is further discussed on the following example.

For the simulation of a turning process, we modelled a hollow shaft represented by a set of particles that is cut by a rigid tool. Figure 17 shows the deformed workpiece and the cutting tool and effects as the formation of a chip and burr are visible.

In Fig. 17, it can once again be observed that the material separates in the region with the highest stretches, but the maximum eigenvalue in the critical finite element is of much smaller value than the predicted limit of 4.0. To understand this effect, we want to investigate the eigenvectors corresponding to the maximum eigenvalues in the workpiece. In Fig. 18, the eigenvectors are plotted in every element in the region of interest.

In Sec. 4, it is mentioned that α can be related to the eigenvalues of the right Cauchy–Green tensor as long as the relevant boundary segment is stretched in the same direction as the eigenvectors. However, Fig. 18 shows that the eigenvector in the critical finite element at the tip of the cutting tool and the related boundary segment are not collinear, which is why the following figure compares the scalar stretch of this boundary segment to α.

In Fig. 19, it can be observed that the stretch of the line segment increases until reaching the critical value α. At this point, the deformed boundary segment is of the same size as the diameter of the α-circle. Any further stretch leads to the failure and elimination of this segment.

7 Conclusion

The particle finite element method is a suitable technique for problems with large configurational changes and can be applied to complex simulations in manufacturing where chips and burrs are formed. In the PFEM, the boundary of a set of particles is detected prior to every load step by the α-shape method. This method is named after its crucial parameter α and it can be observed that a variation of this parameter leads to different topologies of the boundary. Taking a closer look at the α-shape method applied to a single boundary segment in the deformed and undeformed configuration, α can be interpreted as a maximum stretch of a boundary segment. A relation to the eigenvalues of strain tensors, such as the right Cauchy–Green tensor can be established to give a continuum-based interpretation of α. It is shown that the eigenstrains can be compared to α if the corresponding eigenvectors are collinear to the boundary segments. This assumption is first validated on a single finite element and then on numerical examples with simple loading conditions. Contour plots of these simulations show the maximum eigenvalue of the right Cauchy–Green tensor, where the color code is limited by $4\alpha^2$. To give a quantitative measure, the stretch of the critical boundary segments is studied and compared to α in respective line plots. With the aid of this concept, we can provide a prediction for a separation of material in particle finite element simulations applied to solid mechanics.

Acknowledgment

The financial support within the International Research Training Group 2057 is gratefully acknowledged.

References

[1] Oñate, E., Idelsohn, S. R., Del Pin, F., and Aubry, R., 2004, "The Particle Finite Element Method—An Overview," Int. J. Comput. Methods, **1**(2), pp. 267–307.
[2] Carbonell, J. M., Oñate, E., and Suárez, B., 2013, "Modelling of Tunnelling Processes and Rock Cutting Tool Wear With the Particle Finite Element Method," Comput. Mech., **52**(3), pp. 607–629.
[3] Sabel, M., Sator, C., and Müller, R., 2014, "A Particle Finite Element Method for Machining Simulations," Comput. Mech., **54**(1), pp. 123–131.
[4] Idelsohn, S. R., Oñate, E., Del Pin, F., and Calvo, N., 2006, "Fluid-Structure Interaction Using the Particle Finite Element Method," Comput. Methods Appl. Mech. Eng., **195**(17–18), pp. 2100–2123.
[5] Edelsbrunner, H., and Mücke, E. P., 1994, "Three-Dimensional Alpha Shapes," ACM Trans. Graphics, **13**(1), pp. 43–72.
[6] Fischer, K., 2000, "Introduction to Alpha Shapes," Department of Information and Computing Sciences, Faculty of Science, Utrecht University, Utrecht, The Netherlands.
[7] Taylor, R. L., 2009, "FEAP—A Finite Element Analysis Program: User Manual," Department of Civil and Environmental Engineering, University of California, Berkley, CA.
[8] Holzapfel, G., 2000, *Nonlinear Solid Mechanics*, Wiley, Graz, Austria.
[9] Bathe, K. J., 1996, *Finite Element Procedures*, Prentice Hall, Cambridge, UK.
[10] Wriggers, P., 2001, *Nichtlineare Finite-Element-Methoden*, Springer Verlag, Hannover, Germany.
[11] Greve, R., 2003, *Kontinuumsmechanik*, Springer Verlag, Darmstadt, Germany.
[12] Lee, E. H., 1969, "Elastic-Plastic Deformation at Finite Strains," ASME J. Appl. Mech., **36**(1), pp. 1–6.